Semiclassical and Quantum Mechanical Calculations of Isotopic Kinetic Branching Ratios for the Reaction of $O(^3P)$ with HD

Gillian C. Lynch, Philippe Halvick, and Donald G. Truhlar

Department of Chemistry and Supercomputer Institute, University of Minnesota, Minneapolis, MN 55455, U.S.A.

Bruce C. Garrett

Chemical Dynamics Corporation, 9560 Pennsylvania Avenue, Suite 106, Upper Marlboro, MD 20772, U.S.A.

David W. Schwenke

NASA Ames Research Center, Mail Stop 230-3, Moffett Field, CA 94035, U.S.A.

Donald J. Kouri

Department of Chemistry and Department of Physics, University of Houston, Houston, TX 77204-5641, U.S.A.

Z. Naturforsch. **44a**, 427–434 (1989); received January 13, 1989

Dedicated to Professor Jacob Bigeleisen on the occasion of his 70th birthday

Tunneling probabilities for the reactions $O + HD \rightarrow OH + D$ and $O + DH \rightarrow OD + H$ have been calculated by semiclassical dynamical methods and compared to accurate quantal calculations for the same potential energy surface. The results are used to test the reliability of variational transition state theory with the least-action semiclassical method for tunneling probabilities for the prediction of intramolecular kinetic isotope effects.

1. Introduction

It is with great pleasure that the present paper is dedicated to Jacob Bigeleisen on the occasion of his seventieth birthday. Bigeleisen's 1949 paper [1] on the treatment of kinetic isotope effects by transition state theory is a classic paper on this subject. As pointed out by Laidler [2], this early treatment essentially contains the theory that is accepted today, although "later treatments have involved improvements in computational methods and refinements in rate theories." Some of these refinements improve our understanding of the assumptions underlying transition state theory, and others improve the reliability of the quantitative results; some contribute in both ways. A recent review [3] summarizes the status of transition state theory for both gas-phase and condensed-phase reactions. One body of work with which our research group has been especially interested involves variational transition state theory and semiclassical tunneling calculations [4 – 46]. The incorporation of generalized transition states, defined by isotope-dependent effective potentials and free energy of activation profiles, and tunneling contributions, involving the same isotope-dependent effective potentials and isotope-dependent tunneling paths, into conventional transition state theory can lead to systematically more reliable predictions of kinetic isotope effects (KIEs) from potential energy surfaces and hence to more reliable inferences of the chemistry and intermolecular forces from observations of KIEs.

Another recent development in chemical dynamical rate theories is the ability to calculate accurate quantum mechanical reaction probabilities and cross sections by linear algebraic variational solutions of the Schroedinger equation, at least for simple enough systems [47 – 54]. In the present paper we apply both semiclassical tunneling calculations and linear algebraic variational methods to the same intramolecular kinetic isotope effect, namely

$$O(^3P) + HD \begin{cases} \nearrow OH + D & \text{(R1)} \\ \searrow OD + H, & \text{(R2)} \end{cases}$$

Reprint requests to Dr. D. G. Truhlar, Department of Chemistry and Supercomputer Institute, University of Minnesota, Minneapolis, MN 55455, U.S.A.

0932-0784 / 89 / 0500-0427 $ 01.30/0. – Please order a reprint rather than making your own copy.

on the same potential energy surface. This allows a direct test of the semiclassical method, which can be applied to a variety of kinetic isotope effects too complicated for accurate solutions of the Schroedinger equation, e.g., reactions of polyatomics [55 – 57] and reactions at surfaces [58 – 61].

2. Theory

We use a model in which the reaction occurs on a single Born-Oppenheimer potential energy surface. The potential energy surface is a modified London-Eyring-Polanyi-Sato-type [62] surface, parameterized originally by Johnson and Winter [63] and modified by Schatz [64]. This surface, denoted JWS, is assumed to be a good representation of the lowest-energy potential surface for (R1) and (R2). Electronic adiabaticity is assumed for both reactions, and contributions from higher energy surfaces are assumed to be negligible. These assumptions are made for both the approximate and the accurate calculations and therefore do not cause any error in the comparison of the two calculations. No dimensionality reduction is assumed for any of the calculations, i.e., the reactions occur in full three-dimensional space. The masses in atomic units were taken as 2.9163×10^4 for O, 1.8372×10^3 for H, and 3.6743×10^3 for D for both the quantal and semiclassical calculations.

Table 1 summarizes the properties of the JWS surface at the saddle point and the maximum of the ground-state adiabatic potential curve [11] for both reactions (R1) and (R2). In this table, ω_{str} is the frequency of the bound stretching vibration, $\omega^{\ddagger}$ is the imaginary frequency of the reaction coordinate, and ω_{bend} is the frequency of the bending mode. The ODH adiabatic ground-state maximum is 0.1 kcal/mol higher than that for the OHD reaction.

2.1. *Semiclassical Tunneling Calculations*

The present case provides an opportunity to test an approximate method for calculating tunneling probabilities for isotopically substituted chemical reactions in three dimensions against accurate quantum mechanical reaction probabilities. In this article we test the predictions of quantized variational transition state theory [5, 11, 15] (VTST) for ground vibrational state threshold energies and of the least-action-ground-state approximation [27] (LAG) for tunneling probabilities.

Table 1. Saddle point and properties of the maximum of the vibrationally adiabatic ground-state potential curve for OHD and ODH on the JWS potential energy surface.

Species (ABC)		OHD [a]	ODH [b]
Conventional transition state			
$R_{AB}(a_0)$		2.11	2.11
$R_{BC}(a_0)$		1.80	1.80
$V^{\ddagger}$	(kcal/mol)	12.5	12.5
$\hbar\omega_{str}$	(cm^{-1})	1167	1470
$\hbar\omega^{\ddagger}$	(cm^{-1})	1877 i	1491 i
$\hbar\omega_{bend}$	(cm^{-1})	689	574
Adiabatic ground-state maximum			
$R_{AB}(a_0)$		2.11	2.15
$R_{BC}(a_0)$		1.80	1.75
V_a^{AG}	(kcal/mol)	16.3	16.4
ΔV_a^{AG}	(kcal/mol)	10.9	11.0
$\hbar\omega_{str}$	(cm^{-1})	1167	1527
$\hbar\omega_{bend}$	(cm^{-1})	689	587

[a] Transition state for reaction (R 1).
[b] Transition state for reaction (R 2).

In quantized VTST, the reaction path is defined as the minimum energy path through mass-scaled coordinates [4, 56, 65], which is called the MEP, and quantized energy levels for the degrees of freedom orthogonal to the MEP are computed. At the threshold energy of microcanonical transition state theory, the variational transition state is located at the maximum V_a^{AG} of the vibrationally adiabatic ground-state potential curve $V_a^G(s)$ defined by [6, 7, 10, 11, 17]

$$V_a^G(s) = V_{MEP}(s) + \varepsilon^G(s), \tag{1}$$

where s is the distance along the MEP measured from the saddle point, at which $s = 0$ by definition, $V_{MEP}(s)$ is the Born-Oppenheimer potential along the MEP at s, and $\varepsilon^G(s)$ is the sum of the zero point energies of the modes orthogonal to the reaction coordinate at s. $V_{MEP}(s = 0)$ is the classical barrier height, also denoted $V^{\ddagger}$; but the maximum $V_a^G(s)$ occurs at $s = s_*^{AG}$. $\Delta V_a^{AG}(s)$ is defined as

$$\Delta V_a^{AG} = V_a^{AG} - \varepsilon^{RG} = V_a^G(s_*^{AG}) - \varepsilon^{RG}, \tag{2}$$

where ε^{RG} is the zero-point energy of the reactants. The location s_*^{AG} of the variational transition state at threshold also often [5, 6, 66] provides a good indication of where the variational transition state will be at typical temperatures near room temperature, where thermal rate constants are heavily dominated by near-threshold contributions.

The details of the calculational procedures are the same as described elsewhere [11, 27, 28]. The energies of the stretching vibrations are calculated by a WKB

Table 2. Numerical parameters for the quantum mechanical calculations. [a]

	Set 1			Set 2 [b]			Set 3 [b]			Set 4 [b]		
α	O+HD	H+OD	D+OH	O+HD	H+OD	D+OH	O+HD	H+OD	D+OH	O+HD	H+OD	D+OH
N_α	34	70	42	44	82	54						
n_{max}	3	5	3	4	6	4						
j_{max} $(n=0)$	9	16	11	10	17	12						
$(n=1)$	8	14	10	9	15	11						
$(n=2)$	7	12	9	8	13	10						
$(n=3)$	6	10	8	7	11	9						
$(n=4)$	–	8	–	5	9	7						
$(n=5)$	–	4	–	–	6	–						
$(n=6)$	–	–	–	–	4	–						
$N(HO)$	50	50	50				60	60	60			
$N(F)$	680	680	680				956	956	956			
$R^F_{\alpha,1}(a_0)$	1.8	0.9	1.4				1.6	0.8	1.2			
$R^F_{\alpha,N(F)}(a_0)$	15.0	12.0	13.0				16.0	13.0	14.0			
N^{QV}	12	12	12				14	14	14			
$N^{QA}_{\alpha\alpha}$	30	30	30				34	34	34			
m	11	10	10							13	12	12
$R^G_{\alpha,1}(a_0)$	3.3	2.3	3.5							3.25	2.25	3.45
$R^G_{\alpha,N(G)}(a_0)$	5.55	3.92	5.525							5.65	4.01	5.65
$\Delta(a_0)$	0.225	0.18	0.225							0.2	0.16	0.2
c	1.2	1.2	1.2							1.4	1.4	1.4
N^{QGL}	14	14	14				16	16	16			
N^{QR}	12	12	12				13	13	13			
$N^{QA}_{\alpha\alpha'}$	70	70	70				78	78	78			
E	11	11	11				13	13	13			

[a] The notation is as follows:

α	arrangement.
N_α	number of channels for arrangement α.
n_{max}	highest vibrational quantum number.
j_{max}	highest rotational quantum number for each vibrational quantum number.
$N(HO)$	number of harmonic oscillator functions.
$N(F)$	number of points in the finite difference (F.D.) grid.
$R^F_{\alpha,1}$	first point of the F.D. grid (mass-scaled bohr).
$R^F_{\alpha,N(F)}$	last point of the F.D. grid (mass-scaled bohr).
N^{QV}	number of quadrature points over the vibrational functions.
$N^{QA}_{\alpha\alpha}$	number of quadrature points over the angular functions belonging to the same arrangement.
m	number of gaussian functions.
$R^G_{\alpha,1}$	location of the first gaussian function (mass-scaled bohr).
$R^G_{\alpha,N(G)}$	location of the last gaussian function (mass-scaled bohr).
Δ	spacing between gaussian functions (mass-scaled bohr).
c	overlap parameter.
N^{QGL}	number of points in Gauss-Legendre quadrature.
N^{QR}	number of repetition of the Gauss-Legendre quadrature.
$N^{QA}_{\alpha\alpha'}$	number of quadrature points over the angular functions belonging to different arrangements.
E	screening parameter for exchange integrals.

[b] In the parameter sets 2, 3, and 4, when the value of a parameter is not written, it means that the value is the same as in the set 1.

approximation [28]. The rotational partition functions were computed by the quantum mechanical rigid rotor approximation [11]. The energy levels for the bending vibrations were treated by a harmonic-quartic approximation with force constants fit to the actual bending potential with a Taylor-series [11]. The energy levels of the harmonic-quartic potential are obtained using a perturbation-variation method [67]. The comparision of semiclassical tunneling calculations to accurate quantal results will of course test these details of the practical implementation as well as testing the semiclassical approximation *per se*.

The least-action ground-state (LAG) tunneling method [27] is a general method which is applicable to reactions with either small or large reaction-path curvature in mass-scaled coordinates. A curved reaction path causes tunneling paths to be displaced to the concave side of the minimum energy path (MEP) [21, 68 – 70]. The skew angle, defined as the angle between the entrance and exit valleys of the potential energy surface, provides an indicator of the magnitude of the reaction-path curvature; small skew angles generate large reaction-path curvature, and large skew angles generate small reaction-path curvature [21, 27, 29]. Reactions (R1) and (R2) have skew angles of 37.6 degrees and 57.0 degrees respectively, both of which indicate the intermediate curvature range for which the LAG method is expected to be most accurate.

In this method [27] the optimum tunneling path is chosen from a sequence of trial paths by requiring it to have the least imaginary action, thereby leading to the least exponential decay along the path. The set of trial paths for an available energy depends on a single parameter α (where $0 \leqq \alpha \leqq 1$) such that $\alpha = 0$ yields the reference path (the MEP), and $\alpha = 1$ yields the large-curvature tunneling path.

Tunneling probabilities for total energy E, zero total angular momentum, stretching vibrational state n, and bending state i are denoted $P^{\mathrm{LA}}(E, n, i)$, and the vibrationally, rotationally adiabatic potential curves are denoted $V_{\mathrm{a}}(n, i, s)$. For the ground state $P^{\mathrm{LA}}(E, n=0, i=0)$ is called $P^{\mathrm{LAG}}(E)$. To calculate the zero-total-angular-momentum microcanonical cumulative reaction probability for the LAG method, we use the following approximation to the sum over all states of the bending modes for total angular momentum zero [51]:

$$P_{\mathrm{cum}}^{J=0}(E) = P^{\mathrm{LAG}}(E) + \sum_{i \neq 0} P^{\mathrm{LAG}}\{E - V_{\mathrm{a}}[n=0, i, s_*^{\mathrm{AG}}] + V_{\mathrm{a}}[n=i=0, s_*^{\mathrm{AG}}]\}, \tag{3}$$

where s_*^{AG} is the location of the maximum of the adiabatic ground-state potential $V_{\mathrm{a}}^{\mathrm{AG}}(n=i=0, s)$, and the sum is over excited bend states ($i=0$ corresponds to $v_2^l = 0^0$, $i=1$ to 2^0, $i=2$ to 4^0, etc.) which can be compared with the quantum mechanical $J=0$ cumulative reaction probability.

2.2. *Quantum Mechanical Calculations*

The accurate quantum mechanical calculations were carried out by the $\mathscr{L}^2$ generalized Newton variational principle using methods described elsewhere [52–54]. We computed the state-to-state transition probabilities $P_{\alpha n j l \alpha' n' j' l'}$ for a total angular momentum $J=0$ and for five values of the total energy E in the range 10–15 kcal/mol. Here α designates the initial arrangement and n, j, l are the vibrational, rotational, and orbital quantum numbers specifying the initial channel. Primed quantities are used for the final channel. The reaction probabilities for the initial state O + HD ($n=j=0$) were calculated with the summation

$$P_{\alpha'}^{\mathrm{R}} = \sum_{n', j', l'} P_{\alpha=1, n=j=l=0, \alpha' n' j' l'}, \tag{4}$$

where α' is 2 or 3 when the final arrangement is respectively H + OD or D + OH. We also calculated the cumulative reaction probabilities:

$$P_{\alpha'}^{\mathrm{C}} = \sum_{n j l} \sum_{n' j' l'} P_{\alpha=1, n j l \alpha' n' j' l'}. \tag{5}$$

We illustrate the convergence of the $\mathscr{L}^2$ calculations with the four sets of numerical and basis set parameters as specified in Table 2. Set 1 is used for the production runs. Set 2 has a larger channel basis set than set 1, set 3 has different numerical parameters, and set 4 has a larger gaussian basis set. Our convergence criterion is that by increasing the basis sets or by improving the numerical parameters by 10% or more, we should observe a deviation of the probabilities smaller than 1%. The reaction probabilities and the cumulative reaction probabilities computed with the four sets of parameters are presented in Tables 3 and 4. The largest deviation we observe is 0.46%, and this is the deviation of the cumulative reaction probability $P_{\alpha'=3}^{\mathrm{C}}$ between parameter sets 1 and 2, at the total energy $E = 10$ kcal/mol. Tables 5 and 6 show the reaction probabilities and the cumulative reaction probabilities.

Table 3. Convergence check for the reaction probabilities from O + HD ($n=j=0$), at the total energy E. [a]

Parameter set	E (kcal/mol)	$P_{\alpha'=2}^{\mathrm{R}}$	$P_{\alpha'=3}^{\mathrm{R}}$
1	10	2.8859×10^{-8}	3.0777×10^{-9}
2	10	2.8890×10^{-8}	3.0907×10^{-9}
3	10	2.8870×10^{-8}	3.0783×10^{-9}
4	10	2.8868×10^{-8}	3.0776×10^{-9}
1	15	2.4507×10^{-2}	7.5709×10^{-3}
2	15	2.4522×10^{-2}	7.5792×10^{-3}
3	15	2.4510×10^{-2}	7.5705×10^{-3}
4	15	2.4507×10^{-2}	7.5719×10^{-3}

[a] $\alpha'=2$ denotes O + DH → OD + H (R 2), and $\alpha'=3$ denotes O + HD → OH + D (R 1).

Table 4. Convergence check for the cumulative reaction probabilities at the total energy E. [a]

Parameter set	E (kcal/mol)	$P^{c}_{\alpha'=2}$	$P^{c}_{\alpha'=3}$
1	10	7.7883×10^{-8}	7.2378×10^{-8}
2	10	7.7978×10^{-8}	7.2714×10^{-8}
3	10	7.7905×10^{-8}	7.2387×10^{-8}
4	10	7.7902×10^{-8}	7.2391×10^{-8}
1	15	1.3720×10^{-1}	3.0317×10^{-1}
2	15	1.3736×10^{-1}	3.0406×10^{-1}
3	15	1.3720×10^{-1}	3.0309×10^{-1}
4	15	1.3719×10^{-1}	3.0314×10^{-1}

[a] $\alpha'=2$ denotes O + HD → OD + H (R 2), and $\alpha'=3$ denotes O + DH → OH + D (R 1).

Table 5. Reaction probabilities from O + HD ($n=j=0$), at the total energy E. [a]

E (kcal/mol)	E_{rel} (kcal/mol)	$P^{R}_{\alpha'=2}$	$P^{R}_{\alpha'=3}$
10	4.63	2.89×10^{-8}	3.08×10^{-9}
11	5.63	1.32×10^{-6}	2.71×10^{-7}
12	6.63	3.04×10^{-5}	8.80×10^{-6}
13	7.63	4.27×10^{-4}	1.46×10^{-4}
14	8.63	4.00×10^{-3}	1.42×10^{-3}
15	9.63	2.45×10^{-2}	7.57×10^{-3}

[a] $\alpha'=2$ denotes O + DH → OD + H (R 2), and $\alpha'=3$ denotes O + HD → OH + D (R 1).

Table 6. Cumulative reaction probabilities at the total energy E. [a]

E (kcal/mol)	$P^{c}_{\alpha'=2}$	$P^{c}_{\alpha'=3}$
10	7.79×10^{-8}	7.24×10^{-8}
11	4.32×10^{-6}	7.64×10^{-6}
12	1.18×10^{-4}	2.82×10^{-4}
13	1.92×10^{-3}	5.14×10^{-3}
14	2.03×10^{-2}	5.40×10^{-2}
15	1.37×10^{-1}	3.03×10^{-1}

[a] $\alpha'=2$ denotes O + DH → OD + H (R 2), and $\alpha'=3$ denotes O + HD → OH + D (R 1).

3. Discussion

Table 5 shows the ground-state reaction probabilities at total energy E for (R 1) and (R 2). The probabilities for (R 2) are consistently larger than those for (R 1), which agrees with the trend found by Schatz [64]. In contrast, Table 6 shows that for the cumulative reaction probability, which is more directly related to the observable thermally averaged rate constants, the probability of forming OD is greater at the lowest energy, but the probability of forming OH is greater at the higher energies.

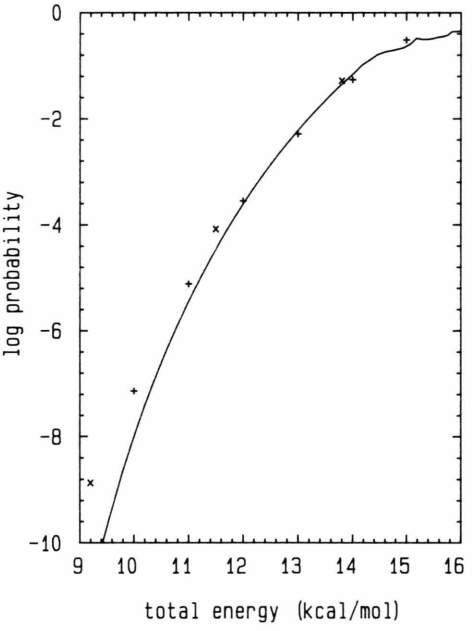

Fig. 1. Logarithm to the base 10 of the $J=0$ cumulative reaction probability vs. total energy for O + HD → OH + D. The semiclassical cumulative reaction probabilities are given as a solid curve. The distorted wave results from [64] are denoted by a ×.

The semiclassical calculations are compared to the accurate quantal ones and to the distorted wave results of Schatz [64] in Figures 1 and 2. The energy range shown in the two figures is below the adiabatic barrier heights for both (R 1) and (R 2), therefore, all cumulative probabilities plotted are for the tunneling region. In Fig. 1 the non-smoothness in the curve of the semiclassical probabilities above 15 kcal/mol seems to result from the classical turning points being located in a region of high reaction-path curvature. Also in Fig. 1, the largest discrepancy between the accurate quantal and the semiclassical cumulative reaction probabilities occurs at a total energy of 10 kcal/mol. At very low energies ($E=10$ kcal/mol to 12 kcal/mol) the semiclassical results are lower than the accurate results, at 13 and 14 kcal/mol the accurate results are lower, and at 15 kcal/mol the semiclassical results are again lower. Figure 2 displays a

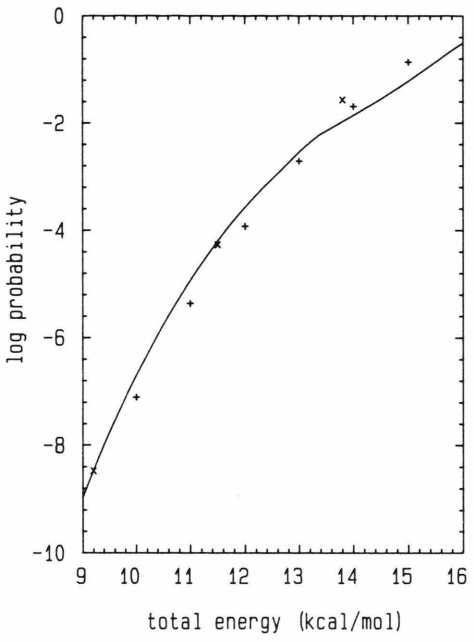

Fig. 2 Same as Fig. 1, except for $O + HD \rightarrow OD + H$.

reverse trend for $E \leqq 12$ kcal/mol, but a similar trend for $E > 12$ kcal/mol. As discussed in the next paragraph, the thermal rate constants at room temperature and above are most sensitive to the latter energy range.

The semiclassical results, like the quantum ones, show a crossover in that the more favored product changes from OD to OH as the energy is increased. The semiclassical transmission coefficients were thermally averaged and combined with improved canonical variational theory to predict thermal rate coefficients at 200 K; the peak in the integrand of the thermal average occurs at $E = 13.39$ kcal/mol for reaction (R 1) and at $E = 12.15$ kcal/mol for reaction (R 2). At these energies, reaction (R 1) is favored and so the OH/OD kinetic isotope effect [i.e., the ratio of the rate constant for (R 1) to that for (R 2)] for this potential surface is predicted to be greater than unity, in fact to be 2.4 at 200 K. Since, however, both the cumulative and ground-state reaction probabilities are smaller for OH than for OD at the lowest energy studied, these calculations predict a nonclassical inversion of the kinetic isotope effect at very low temperature.

Interestingly the cumulative reaction probabilities in Table 6 are much greater than the ground-state reaction probabilities in Table 5. In the semiclassical calculations, however, the sum in (3) is almost totally dominated by the $i = 0$ term. This illustrates that in the transition state region the reactive flux is primarily associated with the ground bending state although many rotational states are important in the reactant and product regions.

The comparison to the distorted wave results [64] for the cumulative reaction probabilities is also shown in Figs. 1 and 2. The distorted wave method is a quantum mechanical approximation that is expected to be especially accurate in the threshold region. Figure 1 confirms this accuracy for reaction (R 1). On the other hand, Fig. 2 shows that for reaction (R 2) the distorted wave results agree better with the semiclassical results (at least at low energy) than with the accurate quantum ones. It is hard to know what these subtle differences mean, but it is encouraging that we now have accurate quantum benchmarks to test quantal approximations as well as semiclassical methods, for kinetic isotope effects.

Figures 1 and 2 show excellent agreement between the semiclassical and the accurate quantum dynamics for both isotopic branches of the reaction. This comparison of semiclassical fixed-energy three-dimensional results with accurate ones is consistent with expectations based on previous comparisons of thermally averaged semiclassical rate coefficients with approximate quantum ones [37] and with comparisons of semiclassical collinear thermal rate constants with accurate quantal ones in the same dimensionality [3]. Since the semiclassical calculations are applicable to systems with many degrees of freedom [29, 55–61] their good agreement with accurate quantal results bodes well for our ability to predict quantum effects on kinetic isotope effects involving tunneling in many systems of interest.

Acknowledgements

The authors are grateful to Kenneth Haug, Yan Sun, and Meishan Zhao for helpful contributions. The semiclassical tunneling calculations were supported in part by the U.S. Department of Energy, Office of Basic Energy Sciences, and the linear algebraic quantum variational calculations were supported in part by the National Science Foundation, NASA, and the Minnesota Supercomputer Institute.

[1] J. Bigeleisen, J. Chem. Phys. **17,** 675 (1949).
[2] K. J. Laidler, Chemical Kinetics, 3rd ed., Harper & Row, New York 1987, p. 427.
[3] D. G. Truhlar, W. L. Hase, and J. T. Hynes, J. Phys. Chem. **87,** 2664 (1983); **87,** 5523 (E) (1983).
[4] B. C. Garrett and D. G. Truhlar, J. Phys. Chem. **83,** 1052 (1979); **87,** 4553 (E) (1983).
[5] B. C. Garrett and D. G. Truhlar, J. Phys. Chem. **83,** 1079 (1979); **87,** 4553 (E) (1987).
[5] B. C. Garrett and D. G. Truhlar, J. Amer. Chem. Soc. **101,** 4534 (1979).
[7] B. C. Garrett and D. G. Truhlar, Proc. Natl. Acad. Sci. USA **76,** 4755 (1979).
[8] B. C. Garrett and D. G. Truhlar, J. Phys. Chem. **83,** 2921 (1979).
[9] B. C. Garrett and D. G. Truhlar, J. Amer. Chem. Soc. **102,** 2559 (1980).
[10] B. C. Garrett and D. G. Truhlar, J. Chem. Phys. **72,** 3460 (1980).
[11] B. C. Garrett, D. G. Truhlar, R. S. Grev, and A. W. Magnuson, J. Phys. Chem. **84,** 1730 (1980); **87,** 4554(E) (1983).
[12] B. C. Garrett, D. G. Truhlar, R. S. Grev, and R. B. Walker, J. Chem. Phys. **73,** 235 (1980).
[13] B. C. Garrett, D. G. Truhlar, R. S. Grev, A. W. Magnuson, and J. N. L. Connor, J. Chem. Phys. **73,** 1721 (1980).
[14] B. C. Garrett, D. G. Truhlar, and A. W. Magnuson, J. Chem. Phys. **74,** 1029 (1981).
[15] D. G. Truhlar and B. C. Garrett, Acct. Chem. Res. **13,** 440 (1980).
[16] B. C. Garrett, D. G. Truhlar, and A. W. Magnuson, J. Chem. Phys. **76,** 2321 (1982).
[17] B. C. Garrett, D. G. Truhlar, and R. S. Grev, in: Potential Energy Surfaces and Dynamics Calculations (D. G. Truhlar, ed.), Plenum, New York 1981, p. 587.
[18] R. T. Skodje, D. G. Truhlar, and B. C. Garrett, J. Phys. Chem. **85,** 3019 (1981).
[19] D. K. Bondi, D. C. Clary, J. N. L. Connor, B. C. Garrett, and D. G. Truhlar, J. Chem. Phys. **76,** 4986 (1982).
[20] N. C. Blais, D. G. Truhlar, and B. C. Garrett, J. Chem. Phys. **76,** 2768 (1982).
[21] R. T. Skodje, D. G. Truhlar, and B. C. Garrett, J. Chem. Phys. **77,** 5955 (1982).
[22] D. C. Clary, B. C. Garrett, and D. G. Truhlar, J. Chem. Phys. **78,** 777 (1983).
[23] N. C. Blais, D. G. Truhlar, and B. C. Garrett, J. Chem. Phys. **78,** 2363 (1983).
[24] B. C. Garrett, D. G. Truhlar, A. F. Wagner, and T. H. Dunning Jr., J. Chem. Phys. **78,** 4400 (1983).
[25] D. K. Bondi, J. N. L. Connor, B. C. Garrett, and D. G. Truhlar, J. Chem. Phys. **78,** 5981 (1983).
[26] D. G. Truhlar, R. S. Grev, and B. C. Garrett, J. Phys. Chem. **87,** 3415 (1983).
[27] B. C. Garrett and D. G. Truhlar, J. Chem. Phys. **79,** 4931 (1983).
[28] B. C. Garrett and D. G. Truhlar, J. Chem. Phys. **81,** 309 (1984).
[29] D. G. Truhlar, A. D. Isaacson, and B. C. Garrett, in: Theory of Chemical Reaction Dynamics (M. Baer, ed.), CRC Press, Boca Raton, FL, 1985, p. 65.
[30] D. G. Truhlar and B. C. Garrett, in: Annual Review of Physical Chemistry, Vol. 35 (B. S. Rabinovich, J. M. Schurr, and H. L. Strauss, eds.), Ann. Rev. Inc., Palo Alto, Calif., 1984, p. 159.
[31] D. G. Truhlar, K. Runge, and B. C. Garrett, in: Twentieth Symposium (International) on Combustion, Combustion Institute, Pittsburgh 1984, p. 585.
[32] S. C. Tucker, D. G. Truhlar, B. C. Garrett, and A. D. Isaacson, J. Chem. Phys. **82,** 4102 (1985).
[33] B. C. Garrett and D. G. Truhlar, J. Phys. Chem. **89,** 2204 (1985).
[34] R. Steckler, D. G. Truhlar, and B. C. Garrett, J. Chem. Phys. **82,** 5499 (1985).
[35] B. C. Garrett, N. Abusalbi, D. J. Kouri, and D. G. Truhlar, J. Chem. Phys. **83,** 2252 (1985).
[36] B. C. Garrett and D. G. Truhlar, Intl. J. Quantum Chem. **29,** 1463 (1986).
[37] B. C. Garrett, D. G. Truhlar, and G. C. Schatz, J. Amer. Chem. Soc. **108,** 2876 (1986).
[38] B. C. Garrett, D. G. Truhlar, J. M. Bowman, A. F. Wagner, D. Robie, S. Arepalli, N. Presser, and R. J. Gordon, J. Amer. Chem. Soc. **108,** 3515 (1986).
[39] B. C. Garrett, D. G. Truhlar, A. J. C. Varandas, and N. C. Blais, Intl. J. Chem. Kinet. **18,** 1065 (1986).
[40] B. C. Garrett, D. G. Truhlar, J. M. Bowman, and A. F. Wagner, J. Phys. Chem. **90,** 4305 (1986).
[41] M. M. Kreevoy, D. Ostovic, D. G. Truhlar, and B. C. Garrett, J. Phys. Chem. **90,** 3766 (1986).
[42] R. Steckler, D. G. Truhlar, and B. C. Garrett, Intl. J. Quantum Chem., Symposium **20,** 495 (1986).
[43] B. C. Garrett and D. G. Truhlar, Intl. J. Quantum Chem. **31,** 17 (1987).
[44] B. C. Garrett, R. Steckler, and D. G. Truhlar, Hyperfine Interactions **32,** 779 (1986).
[45] D. G. Truhlar and B. C. Garrett, J. Chem. Phys. **84,** 365 (1987).
[46] T. Joseph, D. G. Truhlar, and B. C. Garrett, J. Chem. Phys. **88,** 6982 (1988).
[47] K. Haug, D. W. Schwenke, Y. Shima, D. G. Truhlar, J. Zhang, and D. J. Kouri, J. Phys. Chem. **90,** 6757 (1986).
[48] K. Haug, D. W. Schwenke, D. G. Truhlar, Y. Zhang, J. Z. H. Zhang, and D. J. Kouri, J. Chem. Phys. **87,** 1892 (1987).
[49] K. Haug, D. W. Schwenke, Y. Shima, D. G. Truhlar, J. Z. H. Zhang, Y. Zhang, Y. Sun, D. J. Kouri, and B. C. Garrett, in: Science and Engineering on Cray Supercomputers, Proceedings of the Third International Symposium, Minneapolis, Minnesota, September 1987; Cray Research, Minneapolis 1987, p. 427.
[50] J. Z. H. Zhang, D. J. Kouri, K. Haug, D. W. Schwenke, Y. Shima, and D. G. Truhlar, J. Chem. Phys. **88,** 2492 (1988).
[51] J. Z. H. Zhang, Y. Zhang, D. J. Kouri, B. C. Garrett, K. Haug, D. W. Schwenke, and D. G. Truhlar, Faraday Discuss. Chem. Soc. **84,** 371 (1987).
[52] D. W. Schwenke, K. Haug, D. G. Truhlar, Y. Sun, J. Z. H. Zhang, and D. J. Kouri, J. Phys. Chem. **91,** 6080 (1987).
[53] D. W. Schwenke, K. Haug, M. Zhao, D. G. Truhlar, Y. Sun, J. Z. H. Zhang, and D. J. Kouri, J. Phys. Chem. **92,** 3202 (1988).
[54] D. W. Schwenke, M. Mladenovic, M. Zhao, D. G. Truhlar, Y. Sun, and D. J. Kouri, to be published in the proceedings of the NATO Advanced Research Workshop, Supercomputer Algorithms for Reactivity, Dynamics, and Kinetics of Small Molecules, Colombella di Perugia, Italy, August 30–September 3, 1988, D. Reidel, Dordrecht, Holland.
[55] D. G. Truhlar, A. D. Isaacson, R. T. Skodje, and B. C. Garrett, J. Phys. Chem. **86,** 2252 (1982); **87,** 4554(E) (1983).
[56] A. D. Isaacson and D. G. Truhlar, J. Chem. Phys. **76,** 1380 (1982).
[57] T. Joseph, R. Steckler, and D. G. Truhlar, J. Chem. Phys. **87,** 7036 (1987).
[58] J. G. Lauderdale and D. G. Truhlar, J. Amer. Chem. Soc. **107,** 4590 (1985).

[59] J. G. Lauderdale and D. G. Truhlar, Surf. Sci. **164,** 558 (1985).
[60] T. N. Truong and D. G. Truhlar, J. Chem. Phys. **88,** 6611 (1988).
[61] T. N. Truong, G. Hancock, and D. G. Truhlar, Surf. Sci., submitted.
[62] S. Sato, J. Chem. Phys. **23,** 592 (1955).
[63] B. R. Johnson and N. W. Winter, J. Chem. Phys. **66,** 4116 (1977).
[64] G. C. Schatz, J. Chem. Phys. **83,** 5677 (1985).
[65] D. G. Truhlar and A. Kuppermann, J. Amer. Chem. Soc. **93,** 1840 (1971).
[66] B. C. Garrett and D. G. Truhlar, J. Amer. Chem. Soc. **101,** 5207 (1979).
[67] D. G. Truhlar, J. Molec. Spectr. **38,** 415 (1971).
[68] R. A. Marcus, J. Chem. Phys. **45,** 4493 (1966).
[69] R. A. Marcus, J. Chem. Phys. **49,** 2617 (1969).
[70] R. A. Marcus and M. Coltrin, J. Chem. Phys. **67,** 2609 (1977).